DOI: 10.61782/fa.2025.0592

FORUM ACUSTICUM EURONOISE 2025

MULTI-FUNCTIONAL RAINBOW TRAPPING FILTERS FOR PARTICLE ACOUSTIC AGGLOMERATION

Teresa Bravo[1*] **Cédric Maury**[2] **Muriel Amielh**[3]
Daniel Mazzoni[3]
[1] Institute for Physical and Information Technologies (ITEFI), Spanish National Research Council (CSIC), Madrid, Spain
[2] Laboratory of Mechanics and Acoustics (LMA CNRS UMR 7031), Marseille, France
[3] Institute of Research on Non-Equilibrium Phenomena (IRPHE CNRS UMR 7342), Marseille, France

ABSTRACT

Moving towards global zero-emissions in transport and energy supply industries would enable to achieve a quieter, cleaner and healthier urban environment, more resilient to climate-change. The World Health Organisation has classified traffic noise as the second most important cause of ill health in Western Europe, behind only air pollution caused by very fine particulate matter. A leverage effect would be to enhance the agglomeration of the released ultrafine and fine particles into larger particles easily filtered out by classic clean air solutions. However, a major, still unsolved, challenge is to do it without requiring intense sound fields or high-drag flow mixing devices prone to increase flow-particle or particle-particle relative motion. Acoustic rainbow trapping filters (RTFs) have been shown to provide solutions for wideband low-frequency sound dissipation. In this work, we aim at exploiting the effective slow sound – small wavelength properties of acoustic metamaterials traversed by a low-speed flow to provoke mixing and nucleation of the convected ultrafine particles. We will explore conditions on the physical parameters of the RTFs and the seeded particles to produce simultaneous sound dissipation and particle agglomeration. The results open up multi-functional objectives to achieve simultaneous aerosol agglomeration, sound attenuation and low drag performance.

[*] ***Corresponding author***: teresa.bravo@csic.es.

Keywords: *rainbow trapping filters; particle agglomeration, sound dissipation.*

1. INTRODUCTION

Seven million persons in the world are estimated of being killed by air pollution every year [1]. The release of airborne particulate matters (PM) implies a range of adverse health effects. In particular, the growing concentration of fine particles of diameter lower than 2.5 µm per cubic meter in average per year [2] has a significant economic impact on public health system, and additional efforts have to be made to deeper cuts in emission.

Indoor concentration of particles originating inside or outside buildings relies on particle removal by ventilation filtering systems, that depends strongly on the particle sizes. There is a critical gap in the intermediate size range (0.2-1 µm) where classical filters present a pronounced dip for efficiency [3]. Agglomeration can force the smallest particles to aggregate and the filter can then efficiently capture the largest size components. Numerous applications have been tackled using preconditioning of PM agglomeration by generating ultrasonic standing wave fields. They have shown good performance but need very high levels of acoustic intensity to be efficient [4]. Electrostatic particle agglomerators [5] have also shown a great efficiency, but they also require significant electrical energy consumption to be performant.

In this work we propose a new approach based on the properties of acoustic metamaterials. In particular, we will make use of the "slow sound" generation when acoustic waves propagate in a ducted flow surrounded by a

metamuffler [6-9]. If the effective velocity of the incoming sound wave is progressively reduced to zero, sound waves can be eventually trapped in the meta-structure and the particles suspended in the fluid will oscillate and gradually should agglomerate and increase their sizes. The acoustic performance of the metasilencer is presented in Sec. 2, followed by fundamentals of particle agglomeration in Sec. 3. The simulated results will be analysed in Sec. 4 and we will finish with conclusions and some lines for future work in the last section.

2. ACOUSTICAL MODELLING

2.1 Rainbow trapping filters

Rainbow trapping filters (RTF) are composed of a set of outer cavities with increasing depths that are distributed between the inlet at $x=-L$ towards the outlet at $x=0$, as illustrated in Figure 1. One assumes that such acoustic metamufflers are axisymmetric cylindrical of radius R and length L. Progressive increase of the cavity depths ensures impedance matching and low reflection. It also provides axial variation of the wall impedance, resulting in slow sound and trapping of the incident wave.

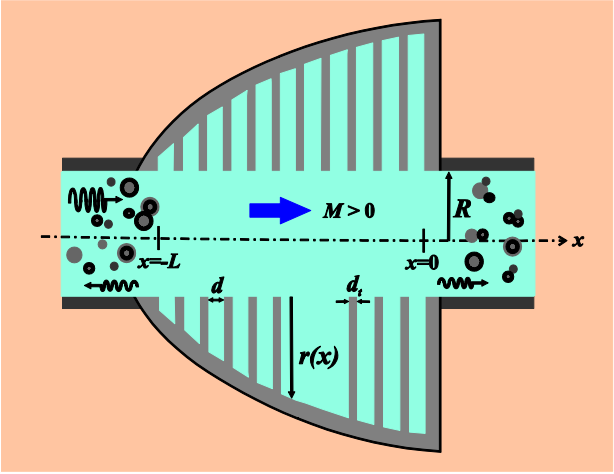

Figure 1. Sketch of a rib-designed rainbow trapping filter traversed by a low-speed flow of grazing Mach number M with an acoustic incident wave travelling along the flow.

A suitable choice of the cavity widths, that can be obtained from optimization of the total dissipation, enables to monitors the amount of visco-thermal losses required to fully dissipate the incident energy trapped within the RTFs.

An RTF with high acoustic performance is characterized by high broadband dissipation, minute reflection and transmission. These properties should be robust when traversed by a low-speed flow. Moreover, the excess friction factor should also be limited, but this aerodynamic constraint will not be considered in the current study. An uncommon design, but with high societal and health impact, is to develop acoustic RTFs that provoke the agglomeration of fine particles into coarser ones that can be readily filtered out by low pressure drop standard filters. The conditions required for these two functionalities will be simulated from transfer matrix modelling for the acoustic part, and from one-dimensional particle transport under drag viscous force for the agglomeration process.

2.2 Transfer matrix modelling

2.2.1 No-flow case

The Transfer Matrix Method (TMM) has been used for the analysis of the widely-opened muffler considering that this device is composed of a set of ring sections separated by air cavities and distributed over an overall length L along the axial dimension. The radii of the air cavities in the fully-opened silencer progressively increase from 0 to R following an expanding power law from the inlet situated at $x=-L$ towards the outlet at $x=0$. Assuming plane wave propagation, the local side-branch volume admittance at $x=x_i$ is given by $Y_{\text{cav},i}=S_{\text{cav}}y(x_i)/Z_0$, with $y(x_i)$ given by Eq. (4) in [6], $S_{\text{cav}}=2\pi Rd$ the cavities entrance area and d their width. Applying continuity of the acoustic pressure and acoustic flow rate across the i^{th} cavity-ring unit leads to the relationship, $[p_i\ u_i]^{\text{T}}=\mathbf{T}_i[p_{i+1}\ u_{i+1}]^{\text{T}}$, between the pressure and volume velocity fields at the input interface $[p_i\ u_i]^{\text{T}}$ and those at the output interface $[p_{i+1}\ u_{i+1}]^{\text{T}}$, with $\mathbf{T}_i$ the associated transfer matrix given by

$$\mathbf{T}_i=\begin{bmatrix}\cos(k_0d) & \mathrm{j}\dfrac{Z_0}{S}\sin(k_0d)\\ \mathrm{j}\dfrac{S}{Z_0}\sin(k_0d) & \cos(k_0d)\end{bmatrix}\times \begin{bmatrix}\cos(k_0d_t) & \mathrm{j}\dfrac{Z_0}{S}\sin(k_0d_t)\\ \mathrm{j}\dfrac{S}{Z_0}\sin(k_0d_t) & \cos(k_0d_t)\end{bmatrix}\times\begin{bmatrix}1 & 0\\ Y_{\text{cav},i} & 1\end{bmatrix} \tag{1}$$

The overall transfer matrix $\mathbf{T}$ between the inlet and the outlet satisfies $[p_1\ u_1]^{\mathrm{T}} = \mathbf{T}[p_{N+1}\ u_{N+1}]^{\mathrm{T}}$ and is expressed as the product of the transfer matrices, $\mathbf{T} = \prod_{i=1}^{N} \mathbf{T}_i = \begin{bmatrix} T_{11} & T_{12} \\ T_{21} & T_{22} \end{bmatrix}$. The expressions for the reflection and transmission coefficients are given by

$$\begin{cases} r = \dfrac{(T_{11} + z_0 T_{12}) - (T_{21} + z_0 T_{22})}{(T_{11} + z_0 T_{12}) + (T_{21} + z_0 T_{22})} \\ t = \dfrac{1 + r}{T_{11} + z_0 T_{12}} \end{cases}. \tag{2}$$

with $z_0 = S/Z_0$ and $S = \pi R^2$. The Johnson-Champoux-Allard-Lafarge model of visco-thermal losses inside the cavities has been used. The power dissipated by the ABH then reads $\eta = 1 - |r|^2 - |t|^2 = \alpha - \tau$ with α the absorption coefficient and τ the transmission coefficient. The transmission loss (TL) is defined as $\mathrm{TL(dB)} = -10\log_{10}(\tau)$.

2.2.2 Low-speed flow effects

The transfer matrix given by Eq. (1) for each cavity cell is extended to account for the convective and dissipative effects of the mean flow on the cell duct sections as well as for the grazing flow effect on the input impedance of the side-branch cavity [10]. It leads to the transfer matrix [11]

$$\widetilde{\mathbf{T}}_L = \mathrm{e}^{-\mathrm{j}M\tilde{k}L} \begin{bmatrix} \cos(\tilde{k}L) & \mathrm{j}\dfrac{Z_0}{S}\sin(\tilde{k}L) \\ \mathrm{j}\dfrac{S}{Z_0}\sin(\tilde{k}L) & \cos(\tilde{k}L) \end{bmatrix}, \tag{3}$$

for a section of length L traversed by a flow at Mach number $M = U/c_0$ with U the mean flow velocity. The duct wavenumber reads $\tilde{k} = (k_0' - \mathrm{j}FM/4R)/(1 - M^2)$ in which k_0' accounts for visco-thermal losses in the duct and $FM/4R$ for the dispersion induced by the turbulent flow, $F = 0.0072 + 0.612\,\mathrm{Re}^{-0.35}$ ($\mathrm{Re} < 4.10^5$) being the Froude's friction factor and $\mathrm{Re} = 2UR\rho_0/\eta$ the ducted flow Reynolds number. Eq. (3) generalizes the two first transfer matrices related in Eq. (1) to sections of length $L = d$ and d_t respectively. Coupling between the ducted flow and the *i*th sidebranch cavity is described by the transfer matrix [11]

$$\widetilde{\mathbf{T}}_{\mathrm{cav},i} = \frac{1}{1 + 2M\widetilde{Y}_{\mathrm{cav},i} z_0^{-1}} \times \begin{bmatrix} 1 + M\widetilde{Y}_{\mathrm{cav},i} z_0^{-1} & M^2 \widetilde{Y}_{\mathrm{cav},i}^2 z_0^{-2} \\ \widetilde{Y}_{\mathrm{cav},i} & 1 + M\widetilde{Y}_{\mathrm{cav},i} z_0^{-1} \end{bmatrix}, \tag{4}$$

so that $\mathbf{T}_i$ in Eq. (1) is replaced by $\widetilde{\mathbf{T}}_i = \widetilde{\mathbf{T}}_d \widetilde{\mathbf{T}}_{d_t} \widetilde{\mathbf{T}}_{\mathrm{cav},i}$. $\widetilde{Y}_{\mathrm{cav},i}$ accounts for the effects of grazing flow on the *i*th cavity input impedance. It can be expressed as [12]

$$\widetilde{Y}_{\mathrm{cav},i} = \frac{1 - M_c H(k_c s)}{Y_{\mathrm{cav},i}^{-1} - 2\dfrac{Z_0}{S_{\mathrm{cav}}} \dfrac{k_0 d}{\pi} \left(1 + \dfrac{\pi d}{4R_i}\right) \dfrac{H(k_c s)}{k_c s}}, \tag{5}$$

in terms of $H(x) = J_0(x)(J_0(x) - \mathrm{j}J_1(x))^{-1}$, $k_c = \omega/U_c$ being the convective wavenumber and $M_c = U_c/c_0$ the convective Mach number with $U_c \approx 0.23\,U$, $R_i = \sqrt{dr(x_i)/\pi}$ and $s = d/2$. The Bessel function terms in H account for the effect of vorticity shed from the cavity upstream edge. Note that Eq. (5) has been derived from linearized perturbation theory [12] assuming a low Mach number flow ($M < 0.3$) and a negligible mean shear across the cavity slit, thereby ruling out any shear layer instability effects.

3. PARTICLE AGGLOMERATION MODELLING

We consider a one-dimensional flow of mean velocity V_a along which propagates an acoustic wave that produces fluid oscillations given by $V_{ac}\sin(k_x x - \omega t)$, so that the total flow velocity reads

$$v_f(x,t) = V_a - V_{ac}\sin(k_x x - \omega t), \tag{6}$$

with $k_x = \omega/c_x$ the acoustic wavenumber and c_x the axial phase speed of the acoustic wave. Assuming that the particle density ρ_p is much greater than the fluid density ρ_0, the effects of inertial and added-mass forces are ignored and only the viscous drag force F_d holds. The equation for particle velocity v_p then reads [13]

$$\frac{dv_p}{dt} = F_d = \frac{1}{St}(v_f - v_p), \tag{7}$$

with $St = \dfrac{\rho_p \omega D_p^2}{18\eta}$ the Stokes number. D_p is the particle diameter. This equation is valid considering a small Stokes number, $St << 1$, meaning that the particles diameter should be small. The condition is achieved for fine ($D_p \leq 2.5\,\mu\text{m}$) and ultrafine ($D_p \leq 0.1\,\mu\text{m}$) particles. It is also required that the particle Reynolds number, $Re_p = \dfrac{2R_p\rho_0|v_f - v_p|}{\eta} \leq 2$. Eq. (7) can then be written in the form $dv_p/dt = (1/t_0)(v_f - v_p)$ with $t_0 = \dfrac{\rho_p D_p^2}{18\eta}$ the particle response time. We can also make the formulation in a moving frame of reference with the phase speed of the acoustic wave c, and in dimensionless form in the position and time by setting $X = kx_p$ and $\tau = \omega t$ [13, 14]. One gets

$$\frac{\mathrm{d}^2X}{\mathrm{d}\tau^2} + \frac{1}{St}\frac{\mathrm{d}X}{\mathrm{d}\tau} + \frac{U_{ac}}{St}\sin(X) = \frac{U_a - 1}{St}, \qquad (8)$$

with $U_a = V_a/c_x$ and $U_{ac} = V_{ac}/c_x$ the dimensionless acoustic and flow velocities. A change of variables can be done such as $\tau' = \tau\sqrt{U_{ac}/St}$, leading to the following equation,

$$\frac{\mathrm{d}^2X}{\mathrm{d}\tau'^2} + \alpha\frac{\mathrm{d}X}{\mathrm{d}\tau'} + \sin(X) = \beta, \qquad (9)$$

with $\alpha = 1/\sqrt{U_{ac}St}$ and $\beta = (U_a - 1)/U_a$. These two parameters control particle agglomeration. The second-order differential equation, Eq. (9), governing the transport of particles under a viscous drag force is solved by a finite-difference Runge-Kutta single-step scheme [15].

4. SIMULATION RESULTS

4.1 Acoustic performance

The acoustical performance of a RTF whose total dissipation has been optimized in plane wave regime [6] are now determined from the transfer matrix formulation presented in Sec. 2.2. It corresponds to a cylindrical rib-designed silencer of radius $R = 0.047\,\text{m}$ and length $L = 0.15\,\text{m}$, comprising a set of $N = 20$ annular cavities of axial width $d = 0.0035\,\text{m}$ separated by ring walls of thickness $d_t = 0.004\,\text{m}$, leading to a wall porosity $\sigma = d/(d + d_t) = 47\,\%$. The optimal rate of increase of the cavity depths is found to be $m = 1.8$. Figure 2 presents the simulated results for the dissipation, reflection and transmission loss power spectra up to the duct cut-on frequency 2142 Hz.

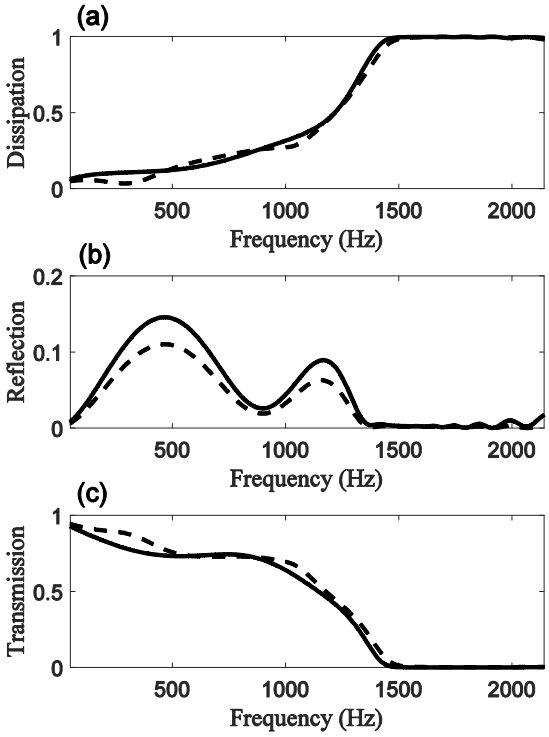

Figure 2. Dissipation (a), reflection (b) and transmission (c) coefficients of a rainbow trapping silencer in the no-flow case (plain) and when traversed by a low-speed grazing flow (dashed) with bulk velocity 20 m.s^{-1}.

Such optimized RTF silencer achieves near-unit dissipation as from 1500 Hz up to the duct cut-on frequency, as seen from Fig. 2(a). The optimization process led to cavity widths with a sufficient amount of visco-thermal losses so that the activated RTF cavity resonances are able to merge and fully dissipate the incident energy over this broad bandwidth. It is accompanied by near-zero reflection that stays below 0.1% over this efficiency range [Fig. 2(b)]. This is caused by the progressive increase of the cavity depths that ensures excellent impedance matching above 1500

Hz. The high dissipative performance result in a minute transmission coefficient above 1500 Hz [Fig. 2(c)]. Figure 3 shows that it translates into high TL values that stays above 27 dB as from 1500 Hz and with a maximum value of 32dB at 1700 Hz. The simulation performance of RTF silencers by the transfer matrix method has been validated against finite element simulations and impedance tube measurements in the no-flow case [6] and against wind-tunnel measurements when traversed by a low-speed flow [10]. The influence of a grazing flow on the acoustical performance of the optimized RTF silencer is also assessed in Figs. 2 and 3 assuming a low-speed bulk velocity of 20 m.s^{-1} (related to a Mach number of 0.06).

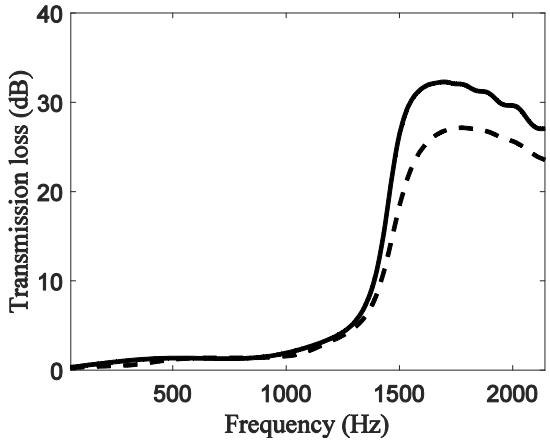

Figure 3. Transmission loss (dB) spectra of a rainbow trapping silencer in the no-flow case (plain) and when traversed by a low-speed grazing flow (dashed) with bulk velocity 20 m.s^{-1}.

As seen in Fig. 1, downstream propagation conditions (DPC) hold in which both the incident wave and the flow travel along the same direction from the inlet to the outlet of the silencer. Such low speed flows produce small effects on the acoustical performance, as seen in Fig. 2. From Fig. 2(a), one observes a moderate upshift (by 40 Hz) of the dissipation spectrum with the near-unit values above 1500 Hz hardly affected by the low-speed flow. The flow influence is mostly noticeable in Fig. 3 with a similar upshift by 40 Hz of the TL bump, but with a decrease by 5 dB of the maximum TL value. This is caused by a decrease of the wall-cavity reactance induced by the flow under DPC as the flow speed increases. A second flow effect is the increase of the wall-cavity resistance under DPC with the flow Mach number. Therefore, the cavity resonances activated over the RTF efficiency bandwidth become slightly over-damped due to the flow effect. This limits the ability of the sound wave to enter the wall cavities and results in a higher transmission and a lower TL. Note that the TL is very sensitive to small amounts of excess damping. Figure 2(b) shows that the impedance matching and reflection properties are weakly modified by the flow.

Of interest is to examine the axial variation of the acoustic velocity within the RTF at different frequencies in plane wave regime: out of the RTF efficiency range (600 Hz), at the onset (1400 Hz) and within (1800 Hz) the RTF high performance bandwidth. The results simulated by the transfer matrix model are illustrated in Fig. 4 with and without flow.

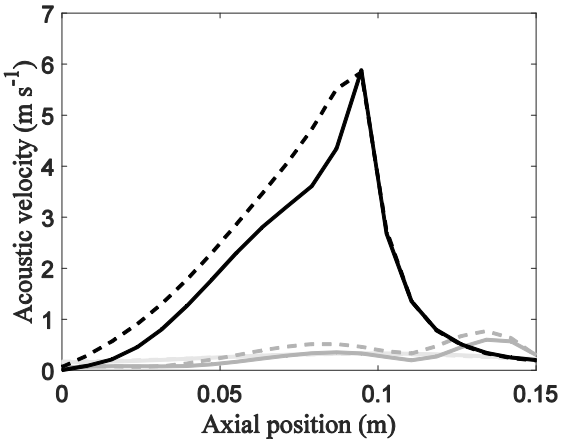

Figure 4. Axial variation of the acoustic velocity within a rainbow trapping filter at 600 Hz (light grey), 1400 Hz (grey) and 1800 Hz (black) in the no-flow case (plain) and when traversed by a low-speed grazing flow (dashed) with bulk velocity 20 m.s^{-1}.

At 600 Hz, the acoustic velocity weakly varies around 0.2 m.s^{-1} (132 dB) along the RTF which is rather inefficient at this frequency. At 1400 Hz, the deepest cavity is about to be activated. Therefore, Fig. 4 shows a slight bump of acoustic velocity around 0.6 m.s^{-1} towards the RTF outlet. At 1800 Hz, the twelfth acoustic cavity (numbered from one to twenty from the inlet to the outlet) is resonant. It results in a significant peak of acoustic velocity at its axial position with a steep (resp. smooth) decay towards the downstream (resp. upstream) cavities. The local rate of increase of the downstream

cavities is smaller than that of the upstream cavities, resulting in a greater density of the downstream resonances (with respect to the upstream resonances). The downstream cavities above order 12 are thus partially activated and also contribute to the dissipation of incident energy. This explains the steep decay of acoustic velocity above these cavities. Converting the acoustic velocity into sound pressure levels (SPLs) requires knowledge of the sound speed which, as seen in Sec. 4.2, varies within the RTF due to slow sound effects. The axial variations of the acoustic velocity in Fig. 4 are not drastically modified by the presence of a low-speed flow. The reactance decrease induced by the flow excites cavities with slightly higher resonance frequencies, e.g. the shallower cavities. This results in higher acoustic velocity for the upstream cavities.

4.2 Slow sound effective properties

Calculations of the axial phase speed $c_x(\omega)$ are achieved from analytical expression of the axial wavenumber $k_x(\omega)$ that appears in the linearized momentum conservation equation [6] that governs the propagation of a plane wave within a RTF with gradual axial variation of the wall impedance along the axial direction. It reads

$$\frac{\mathrm{d}^2 p}{\mathrm{d}x^2} + k_x^2 p = 0\,, \tag{10}$$

with

$$k_x = \frac{\omega}{c_x} = k_0\left[1 - j\frac{y(x)}{k_0 R}\right]^{1/2}, \tag{11}$$

and $y(x)$,defined in Sec. 2.2.1, the specific wall admittance associated to cylindrical cavities of axially increasing depth $r(x) = R\left(1-(-x)^m / L^m\right),\ m>0$.

Axial variations of the phase speed for the sound wave travelling through the RTF is shown in Fig. 5 for various frequencies out, at the onset and within the silencer efficiency range, e.g. at 600 Hz, 1400 Hz and 1800 Hz, respectively. As expected, whatever the frequencies, the axial phase speeds at the inlet of the RTF are equal to the sound speed c_0 of a plane wave travelling in a rigid duct. Within the RTF, the sound wave becomes dispersive and slow sound effects occur. At 600 Hz, $c_x(\omega)$ steadily decays down to 153 m.s^{-1} at the RTF outlet, which is $c_0/2$. At 1400 Hz, the phase speed further decreases and reaches 61 m.s^{-1}, e.g. $c_0/5.6$ at the location of the deepest activated cavity towards the RTF outlet. At 1800 Hz, slow sound effects are even more pronounced with a decay of the phase speed down to 20.5 m.s^{-1}, e.g. $c_0/16.7$, as from 0.09 m, the location of the twelfth activated cavity, until the RTF outlet. A low-speed flow of 20 m.s^{-1} under DPC, simulated by Eq. (5), has a minute effect on the slow sound curves tends to slightly decrease, with only a small uniform decrease of the axial phase speed, whatever the frequency.

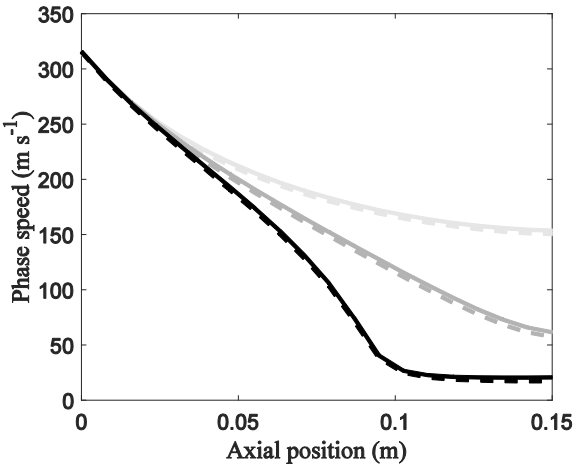

Figure 5. Slow sound effect of an acoustic wave propagating within a rainbow trapping filter at 600 Hz (light grey), 1400 Hz (grey) and 1800 Hz (black) in the no-flow case (plain) and when traversed by a low-speed grazing flow (dashed) with bulk velocity 20 m.s^{-1}.

4.3 Particle axial agglomeration

One considers fine particles of diameter 2µm and density 600 kg.m^{-3}, convected at a mean-flow speed V_a = 20 m.s^{-1} through the acoustically-optimized RTF silencer mounted on a duct. The particles also undergo an oscillatory motion of amplitude V_{ac} and phase speed $c_x(\omega_0)$ due to the slow sound propagation of the acoustic wave at frequency f_0 within the silencer. One assumes monodisperse spherical particles only experiencing viscous drag force induced by the air flow. This is valid for a small Stokes number, defined in Sec. 3, which does not exceed 0.1 at the duct cut-on frequency.

At the initial time, six particles are uniformly distributed over an axial distance of 0.015 m, separated by 3 mm, undergoing the same initial velocity V_a. Eq. (9) is solved using a finite-difference scheme [15]. A condition initially

derived by Sazhin *et al.* [13] for droplet grouping in oscillating flow field, later extended by Zhang *et al.* [14] for acoustic agglomeration in periodic metamaterials, requires that $|\beta| \leq 1$, e.g. $|V_a - c_x| \leq V_{ac}$ for the slow sound to provoke particle agglomeration in an acoustic field with particle velocity V_{ac} convected by mean flow velocity V_a. At 600 Hz, out of the RTF efficiency range, Fig. 6 shows that the trajectories of the particles stay parallel over the length of the silencer, clearly ruling out the occurrence of droplet grouping. Indeed, Fig. 4 showed that V_{ac} stays around 0.2 m.s^{-1} at 600 Hz and Fig. 5 indicates that the smallest phase speed is 153 m.s^{-1} at the RTF outlet. This leads to an agglomeration coefficient β that largely exceeds one, and prevent any grouping of the particles.

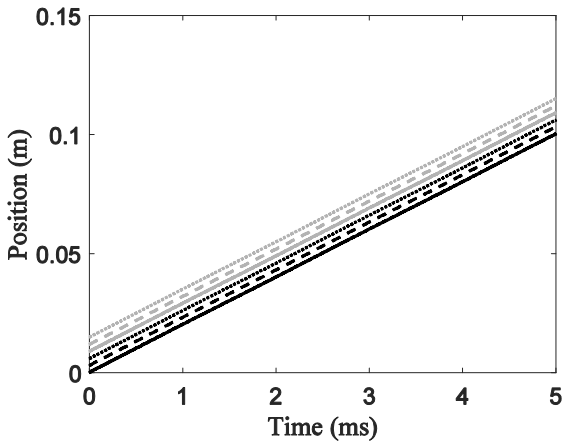

Figure 6. Trajectories of 6 fine particles convected by a low-speed grazing flow with bulk velocity 20 m.s^{-1} within a rainbow trapping filter at 600 Hz, assuming an acoustic phase speed of 153 m.s^{-1} and an acoustic velocity of 0.5 m.s^{-1}.

At 1800 Hz, within the RTF efficiency range, Fig. 7 shows grouping of the six particles into two coarser particles of 6µm diameter, over an axial distance at least 0.09 m apart from the inlet. In this region, at 0.11 m, V_{ac} reaches 2 m.s^{-1} (see Fig. 4) and slow sound effects are prominent with c_x = 20.5 m.s^{-1} (see Fig. 5), resulting in an agglomeration coefficient $\beta = 0.275$ lower than one, that complies with the grouping condition of particles. Figure 8 shows that, if the acoustic velocity is decreased to 0.5 m.s^{-1}, the agglomeration process is still ongoing, but requires a greater duration, and so a longer RTF to ensure slow sound.

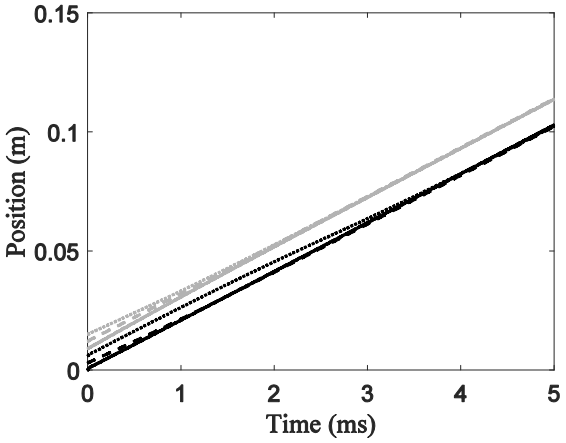

Figure 7. Trajectories of 6 fine particles convected by a low-speed grazing flow with bulk velocity 20 m.s^{-1} within a rainbow trapping filter at 1800 Hz, assuming an acoustic phase speed of 20.5 m.s^{-1} and an acoustic velocity of 2 m.s^{-1}.

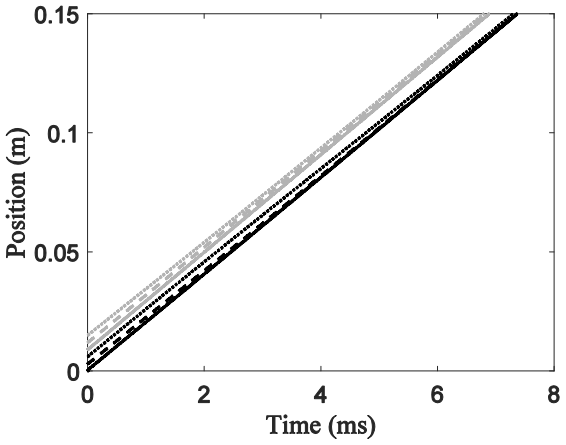

Figure 8. Trajectories of 6 fine particles convected by a low-speed grazing flow with bulk velocity 20 m.s^{-1} within a rainbow trapping filter at 1800 Hz, assuming an acoustic phase speed of 20.5 m.s^{-1} and an acoustic velocity of 0.5 m.s^{-1}.

5. CONCLUSIONS

Conditions under which RTF silencers can achieve multifunctional objectives, namely to fully dissipate the incident sound energy and to agglomerate fine particles into coarser ones, has been discussed in presence of a low-speed flow. Simulations have been carried out based on transfer matrix modelling of the RTF acoustical properties and axial particle transport under viscous drag. It was found that two conditions have to be met to fulfill these objectives. Slow-sound is a pre-requisite to achieve near-unit dissipation over a broad bandwidth, but also for the axial phase speed to get closer from the bulk flow velocity. Moreover, the acoustic velocity within the RTF should be sufficiently high for the agglomeration coefficient to be lower than one and particle grouping to occur at specific axial positions within the RTF. A trade-off should be delineated how to achieve both high attenuation, that creates low acoustic particle velocity, and particle grouping, that requires high particle velocity. This is the object of on-going study as well as the experimental validation of the acoustically-driven particle grouping properties within RTF silencers.

6. ACKNOWLEDGMENTS

This work is part of the project PID2022-139414OB-I00 funded by MCIN/AEI/10.13039/501100011033/ and by "ERDF A way of making Europe". It has also received support from the French government under the France 2030 investment plan, as part of the Initiative d'Excellence d'Aix-Marseille Université - A*MIDEX (AMX-22-RE-AB-157).

7. REFERENCES

[1] Sustainable Development Goal indicator 3.9.1: mortality attributed to air pollution. Geneva: World Health Organization; 2024.

[2] WHO. WHO Ambient Air Quality Database (update 2024). Version 6.1. Geneva, World Health Organization, 2024.

[3] J.T. Hanley, D.S. Ensor, D. D. Smith and L.E. Sparks, "Fractional Aerosol Filtration Efficiency of In-Duct Ventilation Air Cleaners," *Indoor Air,* vol. 4, pp. 169-178, 1994.

[4] G. Reethof, "Acoustic agglomeration of power plant fly ash for environmental and hot gas clean-up," *Noise Control Acoustics,* vol. 110, pp. 552-557, 1988.

[5] W.-Y. Lin, T.-C. Hsiao and B.-L. Hong, "Design and performance of an electrostatic aerosol particle agglomerator," *Journal of the Taiwan Institute of Chemical Engineers*, vol. 107, pp. 110-118, 2020.

[6] T. Bravo and C. Maury: "Broadband sound attenuation and absorption by duct silencers based on the acoustic black hole effect: Simulations and experiments," *Journal of Sound and Vibration*, 561, pp. 117825, 2023.

[7] G. Serra, O. Guasch, M. Arnella, D. Miralles, "Optimization of the profile and distribution of absorption material in sonic black holes," *Mechanical Systems and Signal Processing*, vol. 202, pp. 110707, 2023.

[8] X. Yu, Y. Mi, W. Zhai, L. Cheng, "Principles of progressive slow-sound and critical coupling condition in broadband sonic black hole absorber," *Journal of the Acoustical Society of America*, vol. 154, pp. 2988–3003, 2023.

[9] M. Červenka and M. Bednařík, "On the role of resonance and thermoviscous losses in an implementation of "acoustic black hole" for sound absorption in air," *Wave Motion*, vol. 114, pp. 103039, 2022.

[10] T. Bravo and C. Maury: "Converging rainbow trapping silencers for broadband sound dissipation in a low-speed ducted flow," *Journal of Sound and Vibration*, 589, pp. 118524, 2024.

[11] M. L. Munjal: *Acoustics of Ducts and Mufflers*. 2nd Ed., Hoboken: John Wiley & Sons, 2014.

[12] M. S. Howe, "The influence of grazing flow on the acoustic impedance of a cylindrical wall cavity," *Journal of Sound and Vibration* vol. 67, pp. 533–544, 1975.

[13] S. Sazhin, T, Shakked, V. Sobolev and C. Katoshevski, "Particle grouping in oscillating flows," *European Journal of Mechanics B/Fluids*, 27, pp. 131–149, 2008.

[14] Z. Zhang, M. Abom, H. Boden and M. Karlsson: "Particle Number Reduction in Automotive Exhausts Using Acoustic Metamaterials," *SAE Int. J. Engines* vol. 10 (4), pp. 1-8, 2017.

[15] J. R. Dormand and P. J. Prince, "A family of embedded Runge-Kutta formulae," *J. Comp. Appl. Math.*, Vol. 6, pp. 19–26, 1980.